Accepted Manuscript

Title: Nonlinear free vibration analysis of ultra-thin organic solar plates

Author: Nam V. Nguyen, H. Nguyen-Xuan

DOI: https://doi.org/10.15625/0866-7136/23709

Received date:	31 October 2025
Revised date:	13 November 2025
Accepted date:	08 December 2025
Published online date:	09 December 2025

Please cite this article as: Nguyen, N. V., & Nguyen-Xuan, H. (2025). Nonlinear free vibration analysis of ultra-thin organic solar plates. *Vietnam Journal of Mechanics*. https://doi.org/10.15625/0866-7136/23709

Nonlinear free vibration analysis of ultra-thin organic solar plates

Nam V. Nguyen[a,*], H. Nguyen-Xuan[b]

[a] *Faculty of Mechanical Engineering, Industrial University of Ho Chi Minh City, Ho Chi Minh City, Viet Nam*

[b] *CIRTech Institute, HUTECH University, Ho Chi Minh City, Viet Nam*

Abstract

Organic photovoltaic devices have gained significant attention as promising solutions to global energy challenges, owing to their unique advantages, including lightweight construction, optical transparency, mechanical flexibility, and low production cost. In this context, the present work aims to introduce an efficient computational approach to investigate the nonlinear free vibration characteristics of ultra-thin organic solar panels. To this end, the solar panel structure is modeled as a multilayered plate, in which each functional layer is assumed to be isotropic. The fundamental displacements are formulated using a refined higher-order shear deformation theory with four independent variables, combined with the von Kármán nonlinear strain assumption to capture large-amplitude effects. The nonlinear natural frequencies are subsequently determined using the non-uniform rational B-splines (NURBS)-based isogeometric analysis (IGA) in conjunction with an iterative displacement-control scheme. Several benchmark investigations are performed to validate the accuracy and robustness of the present formulation. Furthermore, the effect of some key factors, including boundary conditions, length-to-thickness ratios, and aspect dimensions, on the nonlinear vibration characteristics is comprehensively investigated in this work. Several significant remarks can be drawn in order to support the design and optimization of ultra-thin organic solar plate structures in practical engineering applications.

Keywords: Nonlinear free vibration; Ultra-thin organic solar cells; Refined higher-order shear deformation theory; Isogeometric analysis.

1. Introduction

Over the past decade, renewable energy resources have emerged as promising solutions to addressing the global challenges, such as climate change, greenhouse gas emissions, as well as environmental pollution. Among these, solar energy based on organic materials has garnered considerable attention owing to notable advantages, such as simple fabrication, low cost, light weight, mechanical flexibility, and excellent material compatibility [1, 2]. It

*Corresponding author.

Email address: nguyennamkt@iuh.edu.vn (Nam V. Nguyen)

is important to note that one of the major challenges facing organic solar cells (OSCs) is their limited operational stability and efficiency, primarily due to the inherently low charge mobility of organic materials [3]. Nevertheless, significant research efforts have been devoted to enhancing the power conversion efficiency (PCE) of organic photovoltaic devices. For instance, using a semi-empirical model combined with a tandem cell strategy, the PCE has been recorded to exceed 17%, as reported in [4]. This significant success can be attributed to advancements in device architecture, the development of active layer materials, as well as optimized fabrication processes [5]. Consequently, OSCs are increasingly being adopted in a wide range of applications, including architecture, automotive engineering, aerospace, and defense technologies [6]. On the other hand, both experimental and numerical studies have been extensively conducted to further advance their performance and practical implementation [7, 8].

In general, solar plates are ultra-thin structures that are highly susceptible to severe mechanical deformations under operational conditions, including bending, folding, twisting, and stretching. Consequently, understanding the fundamental mechanical behavior of solar plates, particularly their vibration characteristics, is of great importance. In the open literature, numerous numerical investigations have been conducted to examine the vibrational behavior of such structures. For example, Li and Liu [9] presented a vibration control study including low-frequency and large-amplitude vibrations of solar panels. Subsequently, dynamic modeling techniques, vibration control theories, and technologies for in-orbit vibration controller design are comprehensively investigated. In addition, the nonlinear dynamic characteristics and vibrational behavior of multilayer organic solar plates are thoroughly investigated by Duc et al. [10] using the analytical solutions. Meanwhile, by applying a Navier-type solution derived from classical plate theory combined with the modified couple stress theory, the size-dependent deflections and natural frequencies of OSC are examined in detail by Li et al. [11]. In another research, Anh et al. [12] introduced analytical solutions to evaluate the nonlinear vibrational behavior of OSCs subjected to wind loads and uniform temperature variations. Furthermore, optimization algorithms are subsequently utilized to determine the maximum natural frequencies in various conditions. In the context of isogeometric analysis, Do et al. [13] investigated the static bending, free vibration, and buckling features of both organic and perovskite solar cells. Several numerical studies on such structures were reported [14–16].

In terms of modern computational frameworks, the isogeometric analysis (IGA) based on NURBS rational functions, pioneered by Hughes et al. [17], has gained significant attention from the scientific community in the past two decades due to computational efficiency as well as seamless integration between computer-aided designing and analysis. The NURBS-based IGA has been extensively applied to investigate the mechanical behavior of a wide range of engineering problems such as structural analysis, thermal responses, contact mechanics, fluid–structure interaction, fracture mechanics, and structural optimization [18, 19]. However, the reviewed literature indicates that the application of IGA to investigate the nonlinear free vibration responses of ultra-thin organic solar plates remains highly limited. Motivated by these findings, the present study aims to present an efficient numerical approach for analyzing the nonlinear free vibration characteristics of ultra-thin organic solar

panels. The fundamental displacements of ultra-thin plates are formulated using a refined higher-order shear deformation theory including four unknowns and the von Kármán nonlinear strain assumption. The nonlinear natural frequencies are subsequently determined using a NURBS-based isogeometric approach combined with a displacement-controlled iterative scheme. This study concentrates on explaining how significant factors such as boundary conditions, length-to-thickness ratios, and aspect dimensions affect the nonlinear vibration characteristics of the organic solar panels. The findings of this work contribute to advancing the understanding and expanding the potential industrial applications of ultra-thin organic solar plate structures.

2. Modeling of organic solar plates

In the current study, the nonlinear free vibration characteristics of ultra-thin organic

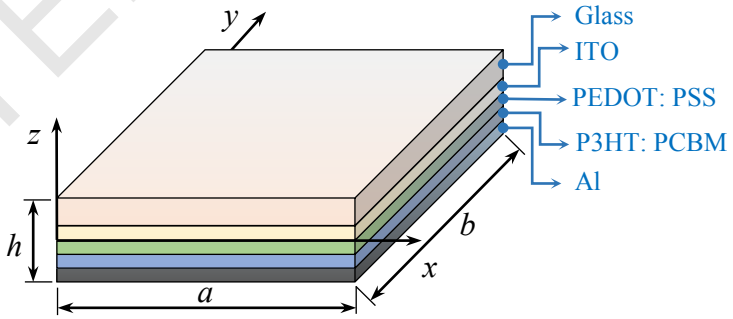

Fig. 1. Schematic representation of the ultra-thin organic solar plates [13].

3. Mathematical expressions

3.1. Refined higher-order shear deformation theory

In the open literature, numerous plate theories have been developed to predict the mechanical behavior of plate structures. Among them, building upon Reddy's higher-order

Table 1. The material properties and thicknesses of ultra-thin organic solar cell [21, 22].

Material	Thickness (μm)	Young's modulus (GPa)	Poisson ratio	Mass density (kg/m^3)
Glass	550	69	0.23	2400
ITO	0.120	116	0.35	7120
PEDOT:PSS	0.050	2.3	0.40	1000
P3HT:PCBM	0.170	6	0.23	1200
Aluminum	0.100	70	0.35	2601

shear deformation theory [25], Senthilnathan et al. [26] introduced a refined higher-order shear deformation theory involving four independent variables. This theoretical model exhibits several notable computational efficiencies, especially when applied to nonlinear problems. Let u_0 and v_0 denote the in-plane displacements along the x and y directions, respectively, while w^b and w^s represent, respectively, the bending and shear parts of transverse displacement. The displacement field of the plate for $z \in [-h/2; -h/2]$ can then be written as follows [26, 27]

$$\begin{cases} u\left(x,y,z\right) = u_0 - zw^b_{,x} + f(z)w^s_{,x}, \\ v\left(x,y,z\right) = v_0 - zw^b_{,y} + f(z)w^s_{,y}, \\ w\left(x,y\right) = w^b + w^s, \end{cases} \tag{1}$$

In the above formulation, the function of $f(z)$ characterizes the distribution of transverse shear strains and stresses through the thickness direction. In the present work, this distribution function is defined as $f(z) = \arctan\left(\sin\left(\frac{\pi}{h}z\right)\right)$, as presented in [28].

The strain–displacement relations derived under the von Kármán assumptions are subsequently formulated as follows

$$\begin{aligned} \boldsymbol{\varepsilon} &= \left\{\boldsymbol{\varepsilon}_{xx}, \boldsymbol{\varepsilon}_{yy}, \boldsymbol{\gamma}_{xy}\right\}^{\mathrm{T}} = \boldsymbol{\varepsilon}_0 + z\boldsymbol{\kappa}_1 + f(z)\boldsymbol{\kappa}_2, \\ \boldsymbol{\gamma} &= \left\{\gamma_{xz}, \gamma_{yz}\right\}^{\mathrm{T}} = [1 + f'(z)]\boldsymbol{\varepsilon}_s, \end{aligned} \tag{2}$$

in which the in-plane, bending and shear strains can be presented as follows

$$\boldsymbol{\varepsilon}_0 = \boldsymbol{\varepsilon}_0^l + \boldsymbol{\varepsilon}_0^{nl}, \boldsymbol{\kappa}_1 = -\begin{Bmatrix} w^b_{,xx} \\ w^b_{,yy} \\ 2w^b_{,xy} \end{Bmatrix}, \boldsymbol{\kappa}_2 = \begin{Bmatrix} w^s_{,xx} \\ w^s_{,yy} \\ 2w^s_{,xy} \end{Bmatrix}, \boldsymbol{\varepsilon}_s = \begin{Bmatrix} w^s_{,x} \\ w^s_{,y} \end{Bmatrix}, \tag{3}$$

In Eq. (3), the linear and nonlinear strains are written as follows

$$\boldsymbol{\varepsilon}_0 = \begin{Bmatrix} u_{0,x} \\ v_{0,y} \\ u_{0,y} + v_{0,x} \end{Bmatrix}, \boldsymbol{\varepsilon}_0^{nl} = \frac{1}{2}\boldsymbol{\Theta}\boldsymbol{\Gamma}, \tag{4}$$

herein,

$$\boldsymbol{\Theta} = \begin{bmatrix} w^b_{,x} + w^s_{,x} & 0 \\ 0 & w^b_{,y} + w^s_{,y} \\ w^b_{,y} + w^s_{,y} & w^b_{,x} + w^s_{,x} \end{bmatrix}, \boldsymbol{\Gamma} = \begin{Bmatrix} w^b_{,x} + w^s_{,x} \\ w^b_{,y} + w^s_{,y} \end{Bmatrix}. \tag{5}$$

By applying Hamilton's principle in conjunction with the weak formulation, the governing weak form for the free vibration analysis of ultra-thin organic solar panels is expressed as follows [28]

$$\int_{\Omega} \delta\boldsymbol{\varepsilon}^T \mathbf{D}^b \boldsymbol{\varepsilon} \mathrm{d}\Omega + \int_{\Omega} \delta\boldsymbol{\gamma}^T \mathbf{D}^s \boldsymbol{\gamma} \mathrm{d}\Omega = \int_{\Omega} \delta\tilde{\mathbf{u}}^T \mathbf{m} \ddot{\tilde{\mathbf{u}}} \mathrm{d}\Omega, \tag{6}$$

in which

$$\begin{aligned} \boldsymbol{\varepsilon} &= \begin{Bmatrix} \boldsymbol{\varepsilon}_0 \\ \boldsymbol{\kappa}_1 \\ \boldsymbol{\kappa}_2 \end{Bmatrix}, \mathbf{D}^b = \begin{bmatrix} \mathbf{A} & \mathbf{B} & \mathbf{E} \\ \mathbf{B} & \mathbf{D} & \mathbf{F} \\ \mathbf{E} & \mathbf{F} & \mathbf{G} \end{bmatrix}, \\ \mathbf{D}^s &= \int_{\frac{-h}{2}}^{\frac{h}{2}} [1 + f'(z)]^2 \begin{bmatrix} C_{55} & 0 \\ 0 & C_{44} \end{bmatrix} \mathrm{d}z, \end{aligned} \tag{7}$$

with

$$[\mathbf{A}, \mathbf{B}, \mathbf{D}, \mathbf{E}, \mathbf{F}, \mathbf{G}] = \int_{\frac{-h}{2}}^{\frac{h}{2}} (1, z, z^2, f(z), zf(z), f^2(z)) \begin{bmatrix} C_{11} & C_{12} & 0 \\ C_{21} & C_{22} & 0 \\ 0 & 0 & C_{66} \end{bmatrix} \mathrm{d}z, \tag{8}$$

in this context, C_{ij}, with $i, j = 1, \ldots, 6$, represents the stiffness coefficients associated with the five functional layers ($k = 1, \ldots, 5$) of the organic solar cell, which can be evaluated as follows

$$\begin{aligned} C_{11}^{(k)} = C_{22}^{(k)} &= \frac{E^{(k)}}{1 - [\nu^{(k)}]^2}, C_{12}^{(k)} = C_{21}^{(k)} = \frac{\nu^{(k)} E^{(k)}}{1 - [\nu^{(k)}]^2}, \\ C_{44}^{(k)} = C_{55}^{(k)} = C_{66}^{(k)} &= \frac{E^{(k)}}{2\,[1 + \nu^{(k)}]}. \end{aligned} \tag{9}$$

In Eq. (6), the quantities $\tilde{\mathbf{u}}$ and $\mathbf{m}$ are formulated, respectively, as follows [29]

$$\tilde{\mathbf{u}} = \begin{Bmatrix} \mathbf{u}_0 \\ \mathbf{u}_1 \\ \mathbf{u}_2 \end{Bmatrix}, \mathbf{m} = \begin{bmatrix} \mathbf{I}_0 & \mathbf{0} & \mathbf{0} \\ \mathbf{0} & \mathbf{I}_0 & \mathbf{0} \\ \mathbf{0} & \mathbf{0} & \mathbf{I}_0 \end{bmatrix}, \mathbf{I}_0 = \begin{bmatrix} I_1 & I_2 & I_4 \\ I_2 & I_3 & I_5 \\ I_4 & I_5 & I_6 \end{bmatrix} \tag{10}$$

herein,

$$\begin{aligned} (I_1, I_2, I_3, I_4, I_5, I_6) &= \int_{-h/2}^{h/2} \rho^{(k)} \left[1, z, z^2, f(z), zf(z), f^2(z)\right] \mathrm{d}z, \\ \mathbf{u}_0 = \begin{Bmatrix} u_0 \\ -w_{,x}^b \\ w_{,x}^s \end{Bmatrix}, \mathbf{u}_1 &= \begin{Bmatrix} v_0 \\ -w_{,y}^b \\ w_{,y}^s \end{Bmatrix}, \mathbf{u}_2 = \begin{Bmatrix} w \\ 0 \\ 0 \end{Bmatrix}. \end{aligned} \tag{11}$$

3.2. Approximation formulations based on NURBS

In general, the primary displacements of ultra-thin organic solar plates can be approximated using the isogeometric approach based on NURBS shape functions as follows [30, 31]

$$\mathbf{u}^h = \begin{Bmatrix} u \\ v \\ w^b \\ w^s \end{Bmatrix} = \sum_{j=1}^{n \times m} \begin{bmatrix} \Phi_j & 0 & 0 & 0 \\ 0 & \Phi_j & 0 & 0 \\ 0 & 0 & \Phi_j & 0 \\ 0 & 0 & 0 & \Phi_j \end{bmatrix} \begin{Bmatrix} u_{0j} \\ v_{0j} \\ w_j^b \\ w_j^s \end{Bmatrix} = \sum_{j=1}^{n \times m} \boldsymbol{\Phi}_j \mathbf{d}_j, \tag{12}$$

in this expression, Φ_j represents the NURBS basis functions, and $\mathbf{d}_j = \left\{ \begin{array}{cccc} u_{0j} & v_{0j} & w_j^b & w_j^s \end{array} \right\}^T$ is the vector of nodal degrees of freedom associated with the j-th control point.

By applying the approximation expression given in Eq. (12), the strain field described in Eq. (3) are then reformulated in a compact form as follows [32]

$$\boldsymbol{\varepsilon} = \boldsymbol{\varepsilon}^l + \boldsymbol{\varepsilon}^{nl} = \sum_{j=1}^{n\times m} \left(\mathbf{B}_j^l + \frac{1}{2}\mathbf{B}_j^{nl} \right) \mathbf{d}_j, \quad \boldsymbol{\varepsilon}_s = \sum_{j=1}^{n\times m} \mathbf{B}_j^s \mathbf{d}_j, \tag{13}$$

where

$$\boldsymbol{\varepsilon}^l = \left\{ \begin{array}{c} \boldsymbol{\varepsilon}_0^l \\ \boldsymbol{\kappa}_1 \\ \boldsymbol{\kappa}_2 \end{array} \right\} = \sum_{j=1}^{n\times m} \mathbf{B}_j^l \mathbf{d}_j, \boldsymbol{\varepsilon}^{nl} = \left\{ \begin{array}{c} \boldsymbol{\varepsilon}_0^{nl} \\ \mathbf{0} \\ \mathbf{0} \end{array} \right\} = \frac{1}{2} \sum_{j=1}^{n\times m} \mathbf{B}_j^{nl} \mathbf{d}_j, \tag{14}$$

with

$$\mathbf{B}_j^l = \left[\begin{array}{c} \mathbf{B}_j^m \\ \mathbf{B}_j^{b1} \\ \mathbf{B}_j^{b2} \end{array} \right], \mathbf{B}_j^{nl} = \left[\begin{array}{c} \boldsymbol{\Theta} \\ \mathbf{0} \\ \mathbf{0} \end{array} \right] \mathbf{B}_j^g, \tag{15}$$

herein, the strain–displacement matrices involved in the formulation are defined as follows

$$\begin{aligned} \mathbf{B}_j^m &= \begin{bmatrix} \Phi_{j,x} & 0 & 0 & 0 \\ 0 & \Phi_{j,y} & 0 & 0 \\ \Phi_{j,y} & \Phi_{j,x} & 0 & 0 \end{bmatrix}, \mathbf{B}_j^{b1} = \begin{bmatrix} 0 & 0 & -\Phi_{j,xx} & 0 \\ 0 & 0 & -\Phi_{j,yy} & 0 \\ 0 & 0 & -2\Phi_{j,xy} & 0 \end{bmatrix}, \\ \mathbf{B}_j^{b2} &= \begin{bmatrix} 0 & 0 & 0 & \Phi_{j,xx} \\ 0 & 0 & 0 & \Phi_{j,yy} \\ 0 & 0 & 0 & 2\Phi_{j,xy} \end{bmatrix}, \mathbf{B}_j^s = \begin{bmatrix} 0 & 0 & 0 & \Phi_{j,x} \\ 0 & 0 & 0 & \Phi_{j,y} \end{bmatrix}, \mathbf{B}_j^g = \begin{bmatrix} 0 & 0 & \Phi_{j,x} & \Phi_{j,x} \\ 0 & 0 & \Phi_{j,y} & \Phi_{j,y} \end{bmatrix}. \end{aligned} \tag{16}$$

By introducing the linear stiffness matrix $\mathbf{K}_l$ and two nonlinear stiffness matrices $\mathbf{K}_{nl}^1$ and $\mathbf{K}_{nl}^2$, the nonlinear governing equation of motion describing the free vibration behavior of ultra-thin organic solar panels is formulated as follows

$$\mathbf{M}\ddot{\mathbf{d}} + \left[\mathbf{K}_l + \mathbf{K}_{nl}^1(\mathbf{d}) + \mathbf{K}_{nl}^2(\mathbf{d}) \right] \mathbf{d} = \mathbf{0}, \tag{17}$$

where the related matrices can be expressed as follows

$$\begin{aligned} \mathbf{K}_l &= \int_\Omega \left(\mathbf{B}^l \right)^T \bar{\mathbf{D}} \mathbf{B}^l \mathrm{d}\Omega, \\ \mathbf{K}_{nl}^1(\mathbf{d}) &= \frac{1}{2} \int_\Omega \left(\mathbf{B}^l \right)^T \bar{\mathbf{D}} \mathbf{B}^{nl} d\Omega + \int_\Omega \left(\mathbf{B}^{nl} \right)^T \bar{\mathbf{D}} \mathbf{B}^l \mathrm{d}\Omega, \\ \mathbf{K}_{nl}^2(\mathbf{d}) &= \frac{1}{2} \int_\Omega \left(\mathbf{B}^{nl} \right)^T \bar{\mathbf{D}} \mathbf{B}^{nl} \mathrm{d}\Omega, \\ \mathbf{M} &= \int_\Omega \hat{\mathbf{R}}^T \mathbf{m} \hat{\mathbf{R}} \mathrm{d}\Omega, \end{aligned} \tag{18}$$

in which $\bar{\mathbf{D}} = \begin{bmatrix} \mathbf{D}_b & \mathbf{0} \\ \mathbf{0} & \mathbf{D}_s \end{bmatrix}$ and $\hat{\mathbf{R}} = \begin{Bmatrix} \mathbf{R}_1 & \mathbf{R}_2 & \mathbf{R}_3 \end{Bmatrix}^T$ with

$$\mathbf{R}_1 = \begin{bmatrix} \Phi_j & 0 & 0 & 0 \\ 0 & \Phi_j & 0 & 0 \\ 0 & 0 & \Phi_j & \Phi_j \end{bmatrix}, \mathbf{R}_2 = \begin{bmatrix} 0 & 0 & -\Phi_{j,x} & 0 \\ 0 & 0 & -\Phi_{j,y} & 0 \\ 0 & 0 & 0 & 0 \end{bmatrix}, \mathbf{R}_3 = \begin{bmatrix} 0 & 0 & 0 & \Phi_{j,x} \\ 0 & 0 & 0 & \Phi_{j,y} \\ 0 & 0 & 0 & 0 \end{bmatrix}. \tag{19}$$

Considering the harmonic vibration problem and employing the Galerkin weighted residual technique to remove the time-dependent component, the eigenvalue equation describing the nonlinear free vibrational characteristics of ultra-thin organic solar plates can be formulated in matrix form as follows [33]

$$\left(-\omega^2\mathbf{M} + \mathbf{K}_l + \frac{8}{3\pi}\mathbf{K}_{nl}^1 + \frac{3}{4}\mathbf{K}_{nl}^2\right)\mathbf{d} = \mathbf{0}, \tag{20}$$

in which ω represents the vibration frequency. It is worth noting that Eq. (20) represents a nonlinear eigenvalue problem, which is typically solved using the displacement control approach, as described in [34, 35]. Accordingly, the linear fundamental frequencies as well as associated vibration modes can be first obtained by neglecting the two nonlinear stiffness matrices, $\mathbf{K}_{nl}^1$ and $\mathbf{K}_{nl}^2$. Subsequently, for a prescribed transverse displacement, the vibration mode is scaled, and the nonlinear stiffness matrices are calculated. The updated eigenvalue problem is then solved to determine the nonlinear frequency and the associated mode shape. This iterative process is repeated until the relative discrepancy between consecutive eigenvalue vectors becomes smaller than the predetermined tolerance of 10^{-5} applied in the present investigation. A detailed flowchart summarizing the solution procedure for the nonlinear free vibration problem can be found in [36].

4. Numerical results

In the following subsection, the nonlinear free vibration responses of thin organic solar plates are examined in detail. The thickness and mechanical properties of the functional layer of the organic solar cells are summarized in Table 1. Unless otherwise specified, all numerical analyses are performed on square solar structures with aspect dimensions of $a = b = 0.05$ m. In addition, the nonlinear-to-linear frequency parameter, expressed as ω_{NL}/ω_L, is then evaluated with respect to various amplitude ratios, $\hat{w} = w_{max}/h$, which serves as an output parameter in this study. Regarding discretization in the NURBS-based IGA framework, a mesh consisting of 11×11 cubic elements is employed to describe the thin organic solar panels. On the other hand, the boundary conditions at the edges are denoted by S, F, and C, corresponding to simply supported, free, and clamped edges, respectively.

4.1. Validation investigation

Due to the scarcity of reference results on the nonlinear free vibrations of ultra-thin organic solar plates, the following two numerical studies are performed to validate the reliability and accuracy of the present approach. In the first investigation, the nonlinear

free vibration characteristics of isotropic square plates with a length-to-thickness ratio of $a/h = 100$ are considered. The material properties of the isotropic plates are specified as Young's modulus $E = 70$ GPa and Poisson ratio $\nu = 0.3$. The results for the nonlinear-to-linear frequency parameter $\hat{w}$ are summarized in Table 2 and compared with those reported in previous studies, namely the analytical solution [37] and the finite element approach [38]. As shown in the Table, a good agreement is achieved between the present findings and the reference results.

Table 2. Nonlinear-to-linear frequency parameter of isotropic plates under SSSS case.

Source	$\hat{w} = w_{max}/h$				
	0.2	0.4	0.6	0.8	1.0
Analytical [37]	1.0168	1.0655	1.1421	1.2415	1.3586
FEM [38]	1.0170	1.0680	1.1490	1.2540	1.3790
Present	1.0143	1.0570	1.1279	1.2267	1.3528

The second validation example concerns the comparison of the linear natural frequency of thin organic solar structures. It is assumed that the ultra-thin organic solar panels are subjected to two types of boundary conditions, specifically SSSS and CCCC cases. In this investigation, the linear natural frequencies are performed in normalized form as follows

$$\overline{\omega} = \omega \frac{a^2}{h} \sqrt{\frac{\rho_G}{E_G}}, \tag{21}$$

in which ρ_G and E_G denote, respectively, the mass density and Young's modulus of the glass layer. The first three normalized natural frequencies of thin organic solar structures corresponding to two a/h ratios are summarized in Table 3. The present findings are compared to those obtained using the HSDT-IGA model, including five variables, reported by Do et al. [13]. As expected, a very close agreement is observed, confirming the accuracy and reliability of the current approach.

Table 3. The first three normalized natural frequencies of thin organic solar plates.

a/h	Source	SSSS			CCCC		
		1	2	3	1	2	3
10	IGA-HSDT [13]	5.6643	13.5100	13.5489	9.7560	18.6533	18.7541
	Present	5.6724	13.5922	13.5922	9.8783	19.1857	19.1857
100	IGA-HSDT [13]	5.8510	14.6208	14.6208	10.6597	21.7266	21.7266
	Present	5.8511	14.6212	14.6212	10.6616	21.7343	21.7343

4.2. Parametric investigation

This subsection is devoted to evaluating the influence of several significant factors, such as boundary conditions, length-to-thickness ratio, and aspect dimensions, on the nonlinear

free vibrational characteristics of thin solar cell structures. In order to evaluate the influence of the boundary constraints at the edges, three representative types of boundary conditions are selected for consideration in this example, specifically SSSS, CSCS, and CCCC. Table 4 summarizes the linear natural frequencies as well as the corresponding nonlinear-to-linear frequency parameters of a thin organic solar plate under various boundary condition cases. This Table reveals that, for all boundary conditions, a gradual increase in the frequency ratio ω_{NL}/ω_L is observed as the amplitude-to-thickness ratio $\hat{w}$ increases. On the other hand, higher natural frequencies are obtained as additional constraints are imposed along the plate edges, increasing from the SSSS to the CSCS and finally to the CCCC case.

Table 4. Linear frequency and nonlinear frequency ratio of solar plates under various boundary conditions.

B.C	ω_L	$\hat{w} = w_{max}/h$					
		0.2	0.4	0.6	0.8	1.0	1.2
SSSS	5.8507	1.0073	1.0290	1.0641	1.1110	1.1683	1.2339
CSCS	8.5783	1.0069	1.0273	1.0603	1.1047	1.1590	1.2218
CCCC	10.6597	1.0072	1.0286	1.0631	1.1096	1.1665	1.2323

In the following numerical study, the influence of the geometrical domain of thin organic solar structures on the nonlinear-to-linear frequency parameter is thoroughly examined. In this specific investigation, it is assumed that thin organic solar panels are subjected to SSSS boundary conditions, while the amplitude-to-thickness ratio may vary from 0.1 to 1.2. Fig. 2 illustrates the variation of the frequency ratio ω_{NL}/ω_L with respect to different aspect ratios a/b. It can be observed that the frequency ratio ω_{NL}/ω_L exhibits a decreasing trend as the aspect ratio a/b increases from 1.0 to 2.0. Moreover, Fig. 2 also reveals that the rise in the nonlinear-to-linear frequency ratio with increasing amplitude-to-thickness ratio $\hat{w}$ is primarily governed by the nonlinear stiffness effect, which is a key characteristic of nonlinear free vibration behavior. On the other hand, Figs. 3 and 4 illustrate the first four linear mode shapes of thin organic solar plates with square ($a/b = 1.0$) and rectangular ($a/b = 2.0$) geometries, respectively, under SSSS boundary conditions. It is worth noting that the corresponding linear natural frequencies are also provided in these figures.

It is well known that the geometrical dimensions of thin organic solar plates have an influence on vibrational behavior. In the final numerical study, the effect of plate length on the nonlinear free vibration characteristics of the solar cell is examined in detail. Accordingly, the square solar plates subjected to two boundary conditions (SSSS and CCCC) are investigated. Three plate lengths, namely $a = 0.02$, 0.06, and 0.10 m, are considered in this example. Table 5 indicates that the normalized linear natural frequencies increase slightly as the plate length increases. In addition, the CCCC boundary condition yields vibrational frequencies approximately twice those of the SSSS case. As expected, an increase in the amplitude-to-thickness ratio $\hat{w}$ results in a corresponding increase in the nonlinear natural frequency.

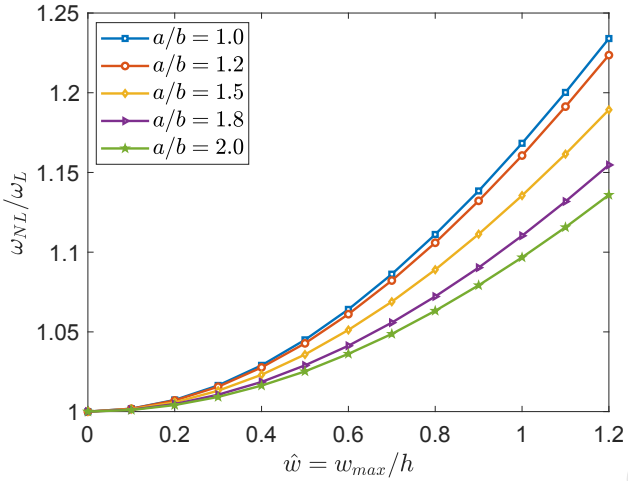

Fig. 2. Variation of the nonlinear-to-linear frequency ratio with varying aspect ratios a/b.

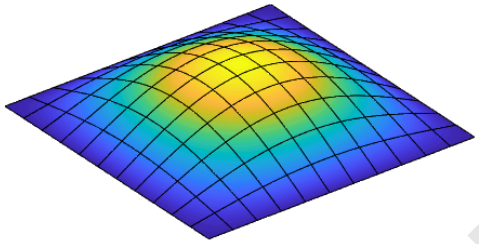

(a) First mode shape, $\omega_L = 5.8507$

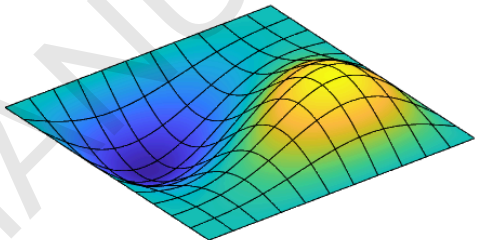

(b) Second mode shape, $\omega_L = 14.6187$

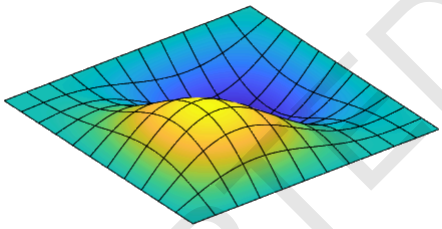

(c) Third mode shape, $\omega_L = 14.6187$

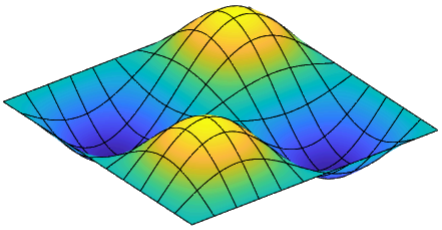

(d) Fourth mode shape, $\omega_L = 23.3757$

Fig. 3. First four linear mode shapes of square solar plates.

5. Conclusions

In this paper, an efficient and robust computational tool was presented in order to study the nonlinear free vibration behavior of ultra-thin organic solar panels. Accordingly, the fundamental mathematical formulations were derived within the NURBS-based isogeometric framework in conjunction with the refined higher-order shear deformation theory. To accurately capture large-amplitude vibration effects, the von Kármán nonlinear strain assumptions are incorporated into the model. In addition, the nonlinear eigenvalue equation was derived using the Galerkin weighted residual method and solved through an iterative

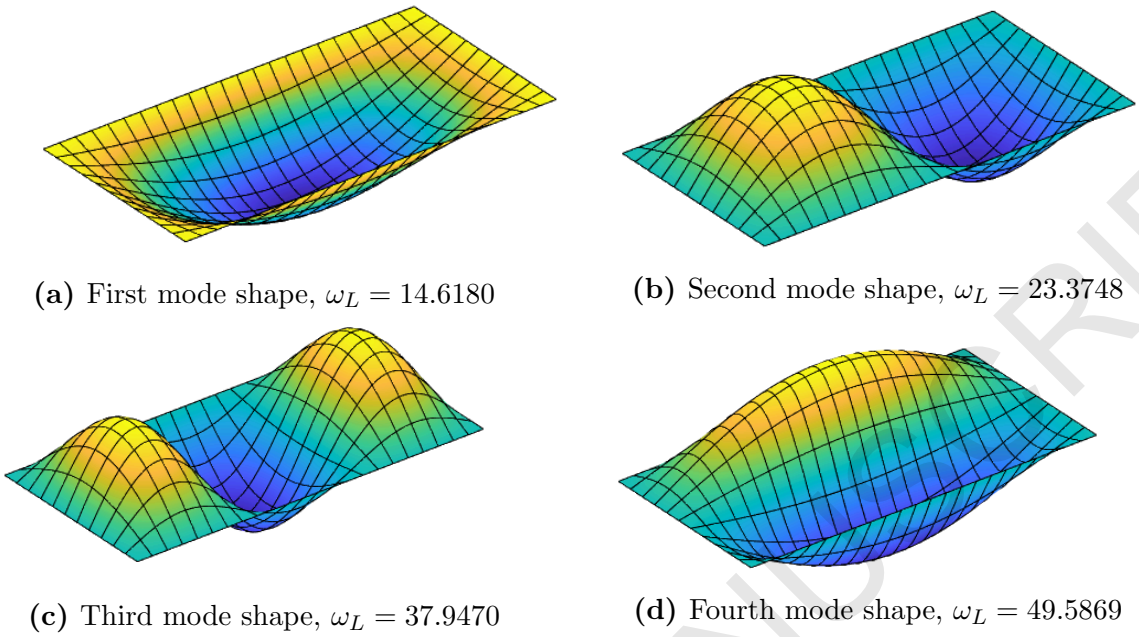

(a) First mode shape, $\omega_L = 14.6180$ **(b)** Second mode shape, $\omega_L = 23.3748$

(c) Third mode shape, $\omega_L = 37.9470$ **(d)** Fourth mode shape, $\omega_L = 49.5869$

Fig. 4. First four linear mode shapes of rectangular solar plates.

Table 5. Linear and nonlinear frequencies of square solar plates with different dimensions.

a	ω_L	$\hat{w} = w_{max}/h$				
(m)		0.2	0.6	1.0	1.4	1.8
			SSSS			
0.02	5.8385	5.8815	6.2139	6.8221	7.6319	8.5719
0.06	5.8514	5.8943	6.2262	6.8361	7.6464	8.5891
0.10	5.8524	5.8954	6.2277	6.8372	7.6476	8.5895
			CCCC			
0.02	10.6027	10.6797	11.2764	12.3768	13.8578	15.6116
0.06	10.6631	10.7403	11.3367	12.4382	13.9189	15.6710
0.10	10.6679	10.7451	11.3410	12.4424	13.9249	15.6758

displacement-control scheme to obtain the nonlinear natural frequencies. Some verification studies are carried out to confirm the robustness and accuracy of the present numerical model. Based on the comprehensive parametric analysis, the following key conclusions are drawn:

- Both linear and nonlinear natural frequencies of ultra-thin organic solar plates were accurately and efficiently calculated via this numerical approach;
- The nonlinear natural frequency exhibited a strong dependence on vibration amplitude, with both the nonlinear frequency and the nonlinear-to-linear frequency ratio increasing as the vibration amplitude increased;

- The boundary conditions applied along the edges, as well as the geometrical parameters, had a significant influence on the nonlinear vibrational characteristics of ultra-thin organic solar plates;
- Finally, to enhance the mechanical performance of ultra-thin solar panels, the integration of bio-inspired lightweight substrates, such as triply periodic minimal surface (TPMS) architectures, represents a highly promising solution. Further investigations into these high-performance structures are recommended for future research.

Acknowledgments

This research is funded by Vietnam National Foundation for Science and Technology Development (NAFOSTED) under grant number 107.02-2023.27.

Declaration of competing interest

The authors declare that they have no known competing financial interests or personal relationships that could have appeared to influence the work reported in this paper.

References

[1] Kumavat PP, Sonar P, Dalal DS. An overview on basics of organic and dye sensitized solar cells, their mechanism and recent improvements. Renewable and Sustainable Energy Reviews 2017;78:1262–1287.

[2] Chen LX. Organic solar cells: Recent progress and challenges. 2019.

[3] Xiong C, Sun J, Yang H, Jiang H. Real reason for high ideality factor in organic solar cells: Energy disorder. Solar Energy 2019;178:193–200.

[4] Meng L, Zhang Y, Wan X, Li C, Zhang X, Wang Y, Ke X, Xiao Z, Ding L, Xia R, et al. Organic and solution-processed tandem solar cells with 17.3% efficiency. Science 2018;361(6407):1094–1098.

[5] Zhu C, Yuan J, Cai F, Meng L, Zhang H, Chen H, Li J, Qiu B, Peng H, Chen S, et al. Tuning the electron-deficient core of a non-fullerene acceptor to achieve over 17% efficiency in a single-junction organic solar cell. Energy & Environmental Science 2020;13(8):2459–2466.

[6] Cardinaletti I, Vangerven T, Nagels S, Cornelissen R, Schreurs D, Hruby J, Vodnik J, Devisscher D, Kesters J, D'Haen J, et al. Organic and perovskite solar cells for space applications. Solar Energy Materials and Solar Cells 2018;182:121–127.

[7] Bartesaghi D, Koster LJA. The effect of large compositional inhomogeneities on the performance of organic solar cells: A numerical study. Advanced Functional Materials 2015;25(13):2013–2023.

[8] Mahmood A, Wang JL. Machine learning for high performance organic solar cells: current scenario and future prospects. Energy & environmental science 2021;14(1):90–105.

[9] Li D, Liu W. Vibration control for the solar panels of spacecraft: Innovation methods and potential approaches. International Journal of Mechanical System Dynamics 2023;3(4):300–330.

[10] Duc ND, Seung-Eock K, Quan TQ, Long DD, Anh VM. Nonlinear dynamic response and vibration of nanocomposite multilayer organic solar cell. Composite Structures 2018;184:1137–1144.

[11] Li Q, Wu D, Gao W, Tin-Loi F, Liu Z, Cheng J. Static bending and free vibration of organic solar cell resting on winkler-pasternak elastic foundation through the modified strain gradient theory. European Journal of Mechanics-A/Solids 2019;78:103852.

[12] Anh VM, Quan TQ, Tran P. Nonlinear vibration and geometric optimization of nanocomposite multilayer organic solar cell under wind loading. Thin-Walled Structures 2021;158:107199.

[13] Do DT, Nguyen AT, Nguyen NV. An isogeometric approach of static, free vibration and buckling analyses of multilayered solar cell structures. International Journal of Mechanics and Materials in Design 2024;20(3):463–479.

[14] Nguyen NV, Tran KQ, Fantuzzi N, Nguyen-Xuan H. A size-dependent nonlinear analysis of perovskite solar panels with FG-CNTR-TPMS substrates. Composite Structures 2025;351:118548.

[15] Nguyen NV, Zur KK, Nguyen-Xuan H. Supersonic flutter characteristics of perovskite solar panels integrated into nature-inspired structures. Thin-Walled Structures 2025;:113358.

[16] Nguyen NV. A four-variable isogeometric approach for flutter analysis of ultra-thin perovskite solar structures. Materials and Emerging Technologies for Sustainability 2025;:2550014.

[17] Hughes TJ, Cottrell JA, Bazilevs Y. Isogeometric analysis: CAD, finite elements, NURBS, exact geometry and mesh refinement. Computer methods in applied mechanics and engineering 2005;194(39-41):4135–4195.

[18] Tran HD, Nguyen BH. An isogeometric sgbem for crack problems of magneto-electro-elastic materials. Vietnam Journal of Mechanics 2017;39(2):135–147.

[19] Gupta V, Jameel A, Verma SK, Anand S, Anand Y. An insight on nurbs based isogeometric analysis, its current status and involvement in mechanical applications. Archives of Computational Methods in Engineering 2023;30(2):1187–1230.

[20] Li Q, Tian Y, Wu D, Gao W, Yu Y, Chen X, Yang C. The nonlinear dynamic buckling behaviour of imperfect solar cells subjected to impact load. Thin-Walled Structures 2021;169:108317.

[21] Li Q, Wang Q, Wu D, Chen X, Yu Y, Gao W. Geometrically nonlinear dynamic analysis of organic solar cell resting on winkler-pasternak elastic foundation under thermal environment. Composites Part B: Engineering 2019;163:121–129.

[22] Li Q, Wu D, Gao W, Tin-Loi F. Size-dependent instability of organic solar cell resting on winkler–pasternak elastic foundation based on the modified strain gradient theory. International Journal of Mechanical Sciences 2020;177:105306.

[23] Shen HS, Li C. Modeling and evaluation for large amplitude vibration and nonlinear bending of perovskite solar cell. Composite Structures 2023;303:116235.

[24] Guo H, Yuan J, Zur KK. Flutter and divergence zones of perovskite solar cell-based panels of aircraft wings in subsonic airflow. Aerospace Science and Technology 2024;145:108841.

[25] Reddy JN. Mechanics of laminated composite plates and shells: theory and analysis. CRC press , 2003.

[26] Senthilnathan N, Lim S, Lee K, Chow S. Buckling of shear-deformable plates. AIAA journal 1987;25(9):1268–1271.

[27] Chung NT, Thu DTN. Static stability study of stiffened functionally graded composite plates reinforced by carbon nanotubes using finite element method. Vietnam Journal of Mechanics 2023;45(3):216–234.

[28] Nguyen-Xuan H, Tran LV, Thai CH, Kulasegaram S, Bordas SPA. Isogeometric analysis of functionally graded plates using a refined plate theory. Composites Part B: Engineering 2014;64:222–234.

[29] Tran LV, Thai CH, Le HT, Gan BS, Lee J, Nguyen-Xuan H. Isogeometric analysis of laminated composite plates based on a four-variable refined plate theory. Engineering Analysis with Boundary Elements 2014;47:68–81.

[30] Cottrell JA, Hughes TJ, Bazilevs Y. Isogeometric analysis: toward integration of CAD and FEA. John Wiley & Sons , 2009.

[31] Thai CH, Nguyen-Xuan H. A simple size-dependent isogeometric approach for bending analysis of functionally graded microplates using the modified strain gradient elasticity theory. Vietnam Journal of Mechanics 2020;42(3):255–267.

[32] Nguyen HX, Atroshchenko E, Nguyen-Xuan H, Vo TP. Geometrically nonlinear isogeometric analysis of functionally graded microplates with the modified couple stress theory. Computers & Structures 2017;193:110–127.

[33] Tao C, Dai T. Isogeometric analysis for size-dependent nonlinear free vibration of graphene platelet reinforced laminated annular sector microplates. European Journal of Mechanics-A/Solids 2021;86:104171.

[34] Mirzaei M, Kiani Y. Nonlinear free vibration of temperature-dependent sandwich beams with carbon nanotube-reinforced face sheets. Acta Mechanica 2016;227(7):1869–1884.

[35] Mohammadzadeh-Keleshteri M, Asadi H, Aghdam M. Geometrical nonlinear free vibration responses of fg-cnt reinforced composite annular sector plates integrated with piezoelectric layers. Composite Structures 2017;171:100–112.

[36] Nguyen NV, Phan DH. Nonlinear free vibration of bi-directional functionally graded porous plates. Thin-Walled Structures 2023;192:111198.

[37] Razavi S, Shooshtari A. Nonlinear free vibration of magneto-electro-elastic rectangular plates. Composite Structures 2015;119:377–384.

[38] Han W, Petyt M. Geometrically nonlinear vibration analysis of thin, rectangular plates using the hierarchical finite element method—i: the fundamental mode of isotropic plates. Computers & Structures 1997;63(2):295–308.